Crystal Structure and Mechanism of the *Staphylococcus cohnii* Virginiamycin B Lyase (Vgb)[†,‡]

Magdalena Lipka,[§,||] Renata Filipek,[§,||] and Matthias Bochtler*[,§,||,⊥]

International Institute of Molecular and Cell Biology, Trojdena Street 4, 02-109 Warsaw, Poland, Max-Planck-Institute of Molecular Cell Biology and Genetics, Pfotenhauerstrasse 108, 01309 Dresden, Germany, and Schools of Chemistry and Biosciences, Cardiff University, Main Building, Park Place, Cardiff CF10 3AT, United Kingdom

Received July 31, 2007; Revised Manuscript Received February 1, 2008

ABSTRACT: The semisynthetic streptogramin antibiotic quinupristin/dalfopristin (trade name Synercid, Aventis Pharma) is a mixture of the A-type streptogramin dalfopristin and the B-type streptogramin quinupristin, a capped hexapeptide macrolactone. Quinupristin/dalfopristin was developed to combat multidrug resistant pathogens, but suffers from its own problems with drug resistance. Virginiamycin B lyase (Vgb) inactivates the quinupristin component of Synercid by lactone ring opening. Remarkably, the enzyme promotes this reaction by intramolecular β-elimination without the involvement of a water molecule. Recently, structures of *S. aureus* Vgb in the presence and absence of substrate were reported and used together with detailed mutagenesis data to suggest a catalytic mechanism. Here, we report an independent determination of the *S. cohnii* Vgb crystal structure and a biochemical characterization of the enzyme. As expected, the *S. cohnii* and *S. aureus* Vgb structures and active sites are very similar. Moreover, both enzymes catalyze quinupristin lactone ring opening with similar rate constants, albeit perhaps with different dependencies on divalent metal ions. Replacement of the conserved active site residues His228, Glu268, or His270 with alanine reduces or abolishes *S. cohnii* Vgb activity. Residue Lys285 in *S. cohnii* Vgb is spatially equivalent to the *S. aureus* Vgb active site residue Glu284. A glutamate but not an alanine residue can substitute for the lysine without significant loss of activity.

Quinupristin/dalfopristin (trade name Synercid, Aventis Pharma), a 70:30 mixture of the A-type streptogramin dalfopristin and the B-type streptogramin quinupristin, has recently been licensed for the treatment of serious and life-threatening infections caused by vancomycin-resistant *Enterococcus faecium* and for complicated skin and soft tissue infections caused by susceptible pathogens, including methicillin-resistant strains of *Staphylococcus aureus* (*1–3*). Orally available successors to the parenterally active Synercid are currently in development (*4*). Quinupristin/dalfopristin targets bacterial ribosomes: its dalfopristin component interferes with the correct positioning of substrates for the ribosomal A- and P-sites, and its quinupristin component blocks access to the tunnel through which nascent peptides would normally travel (*5–7*).

Quinupristin/dalfopristin was developed to combat multidrug resistant pathogens, but suffers from its own problems with drug resistance (*8*). As quinupristin/dalfopristin related streptogramin antibiotics have been extensively used in veterinary medicine for the prevention and treatment of enteric diseases of farm animals (*9*), several resistance mechanisms have evolved and are already characterized at the molecular level: the *vat* and *vga* genes encode a dalfopristin-inactivating acetyltransferase (*10–12*) and an efflux pump for A-type streptogramins (*13, 14*), respectively. The products of *erm* gene are methyltransferases, which modify ribosomes and render them resistant to quinupristin (*15, 16*). Moreover, the *vgb* gene product was found to inactivate B-type streptogramins such as quinupristin by a linearization of the cyclic depsipeptides (*11, 17*).

Originally, Vgb[1] was thought to linearize streptogramin B by a hydrolysis reaction of the ester bond that links a threonine side chain of the linear peptide to the carboxy-terminus. However, a careful examination of the *Streptomyces lividans* and *S. aureus* Vgb catalyzed reactions revealed that the linearization of the depsipeptide proceeds instead by intramolecular β-elimination leading to the formation of an N-terminal dehydrobutyrine group (*18, 19*)

[†] This work was supported by the Polish Ministry of Science and Higher Education (MNiSW, decisions 1789/E-529/SPB/5.PR UE/DZ 600/2002–2005, 158/E-338/SPB/5.PR UE/DZ 19/2003 and PBZ-KBN-88/PO4/2003) and by the Commission of the European Communities, specific RTD program "Quality of Life and Management of Living Resources", QLRT-2001-01250, "Novel non-antibiotic treatment of staphylococcal diseases". R.F. acknowledges the fellowship from the Foundation for Polish Science (FNP). M.B. is grateful for Young Investigator Support from the European Molecular Biology Organization (EMBO) and the Howard Hughes Medical Institute (HHMI).

[‡] The coordinates of the structure reported in this manuscript have been deposited with the PDB with accession code 2QC5.

* To whom correspondence should be adressed. Tel: 0048 22 5970732. Fax: 0048 22 5970715. E-mail: MBochtler@iimcb.gov.pl.

[§] International Institute of Molecular and Cell Biology.

[||] Max-Planck-Institute of Molecular Cell Biology and Genetics.

[⊥] Cardiff University.

[1] Abbreviations: Vgb, virginiamycin B lyase; CMLE, 3-carboxy-*cis,cis*-muconate lactonizing enzyme; BSA, bovine serum albumin; TLC, thin layer chromatography; HyPic, 3-hydroxypicolinic acid; GST, glutathione *S*-transferase; HEPES, 4-(2-hydroxyethyl)-1-piperazineethanesulfonic acid; DMSO, dimethyl sulfoxide; EDTA, diaminoethanetetraacetic acid; IPTG, isopropyl-β-D-thiogalactopyranoside.

10.1021/bi7015266 CCC: $40.75
Published on Web 03/15/2008

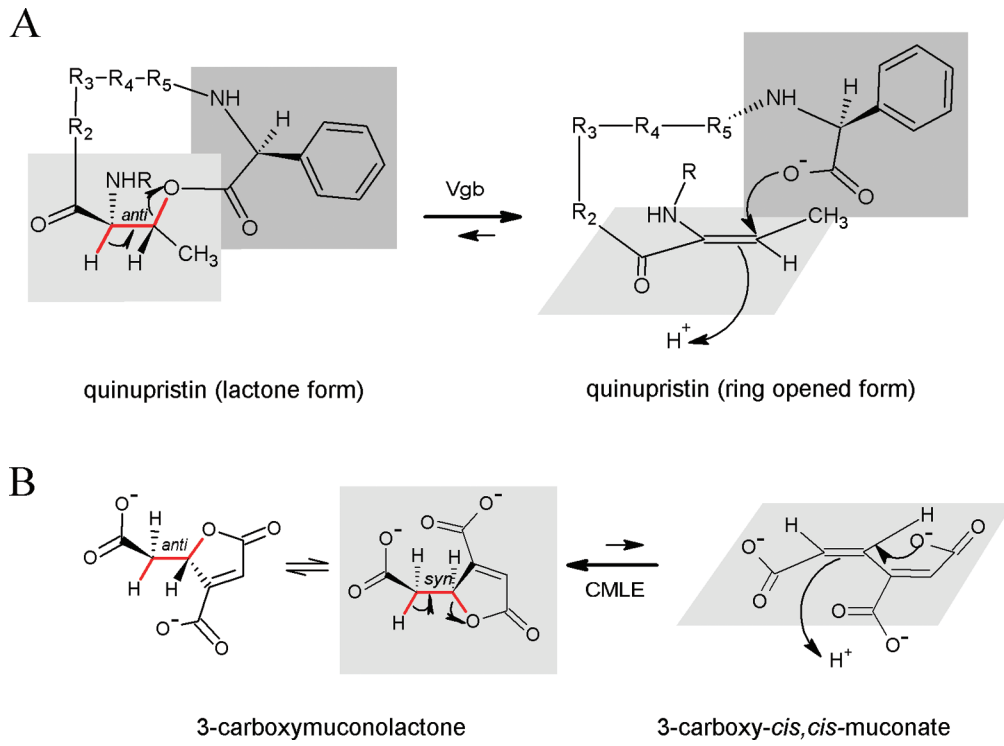

FIGURE 1: Intramolecular elimination reactions. (A) Vgb catalyzed reaction. R is 3-hydroxypicolinyl, R2 is 2-amino-butanoyl, R3 is prolyl, R4 is *N*-methyl-4*N*-dimethylphenylalanyl and R5 is 5-[3-quinuclidinylthiomethyl]-4-oxopipecolyl. Light shading highlights threonyl residue in the quinupristin substrate (left) and dehydrobutyrine group in the ring-opened product (right). Dark shading marks the phenylglycyl residue. Mukhtar et al. have shown that elimination results in the Z-isomer (NHR and CH_3 groups on the same side of the double bond) of ring-opened quinupristin (*19*); therefore, the reaction must be an *anti*-elimination as shown in the figure. (B) *N. crassa* CMLE catalyzed reaction. Reported ^{1}H NMR coupling constants are consistent with the assumption that the dominant conformation of 3-carboxymuconolactone in solution is the one with the bulkiest substituents *anti*-periplanar (far left). A detailed study by Kirby et al. has shown that in the ring-opening direction, CMLE catalyzes a *syn*-elimination, which can only proceed from the less favorable, eclipsed conformation of the muconolactone (*36*).

(Figure 1A). The *S. aureus* Vgb catalyzed reaction proceeds as an *anti*-elimination that is strictly dependent on the presence of divalent metal cations. Although the Vgb catalyzed reaction is remarkable, it is not unprecedented: the 7-bladed β-propeller protein 3-carboxy-*cis,cis*-muconate lactonizing enzyme (CMLE), which equilibrates 3-carboxy-*cis,cis*-muconate and the 3-carboxymuconolactone, catalyzes a similar reaction in the ring-opening direction (*20*) (Figure 1B). However, in contrast to Vgb, CMLE catalyzes a *syn*-elimination reaction and does not require metal ion assistance (*20*). At the outset of this work, CMLE was the closest structurally characterized enzyme to *S. cohnii* Vgb. While this work was in progress, the crystal structures of *S. aureus* Vgb (67% sequence identity to *S. cohnii* Vgb) in the presence and absence of substrate were published (*21*). On the basis of these data and the characterization of a set of *S. aureus* Vgb mutants, a detailed catalytic mechanism was proposed (*21*). Here, we report our independent crystal structure determination of *S. cohnii* Vgb and the analysis of a similar set of active site mutants. Our data confirm the key conclusions of the study of *S. aureus* Vgb, but also indicate that some residues, which are essential for *S. aureus* Vgb mediated catalysis, play only auxiliary roles in *S. cohnii* Vgb.

EXPERIMENTAL PROCEDURES

Quinupristin Purification. Synercid was purchased from Aventis Pharma. Preliminary thin layer chromatography (TLC) experiments (silica gel 60, F254 Merck) were run with methanol as the mobile phase. Dalfopristin migrated close to the solvent front ($R_f \approx 0.83$). Quinupristin did not migrate at all with pure methanol as the mobile phase ($R_f \approx 0$), but could be eluted with a 4:1 mixture of methanol and acetic acid ($R_f \approx 0.24$). Quinupristin spots on TLC plates could be visualized under UV light with a maximum at 254 or at 360 nm. Dalfopristin was visible only under 254 nm illumination.

On the basis of these findings, a preparative separation of quinupristin and dalfopristin was set up. A glass column of height 40 cm and diameter 1.5 cm was packed with silica gel 100 (particle size 0.063 – 0.200 mm, 70–230 mesh, Fluka) in *n*-hexane and loaded with 25 mg of Synercid in 100 μL of methanol. Development of the column with methanol eluted dalfopristin as a yellow solution. Quinupristin was recovered from the column with a 4:1 mixture of methanol and acetic acid and appeared orange. Organic solvents were evaporated under reduced pressure. Dalfopristin was dissolved in 20% DMSO in water, quinupristin in double distilled water. Mass spectrometry confirmed the expected molecular masses.

Cloning. Plasmid pIP1714 (4,978 bp), which confers resistance to streptogramins A and B and the mixture of these compounds, was isolated by Allignet et al. from a *Staphylococcus cohnii* subsp. *cohnii* strain found in the environment of a hospital where pristinamycin was extensively used (*11*). Plasmid pIP1714, which contains the *S. cohnii vgb* gene, was transferred experimentally to *S. aureus*, creating *S. aureus* subsp. *aureus* strain BM12392-I1877, which we

obtained from the Pasteur Institute collection. Lysate of BM12392-I1877 was prepared according to technical information sheet number 12 of the Deutsche Sammlung von Mikroorganismen und Zellkulturen GmbH (unpublished; available on the Internet). Cells were grown to $OD_{600} = 0.6$ in 10 mL BHI medium (Fluka), harvested by centrifugation, resuspended in 0.5 mL solution A (7.5 mM NaCl, 50 mM EDTA at pH 7.0) and incubated with 10 μg of lysostaphin (Sigma) with gentle mixing, first for 0.5 h at 37 °C and then for 0.5 h at 4 °C after the addition of 0.75 mL solution B (0.4% deoxycholate, 0.3 M EDTA at pH 8.0). Insoluble debris was removed by centrifugation. Finally, 1.25 mL of H_2O was added to the supernatant, and the mixture was incubated with 4 μg of RNase at 37 °C for 1 h. One microliter of template was used to amplify the *vgb* gene by standard PCR (Pfu polymerase, Fermentas) with *Hin*dIII and *Xho*I cleavable primers. Using these restriction sites, the fragment was then cloned into pGEX-5T (*22*). The resulting plasmid pGEX-5T-Vgb was ampicillin-selectable, and directed the heterologous expression of Vgb with an N-terminal, thrombin-cleavable GST-tag in *Escherichia coli*. Site directed mutations in the expression construct were introduced by the QuickChange method (Stratagene), essentially according to the manufacturer's protocol, but with either Pfu Plus polymerase (EURx) or WALK polymerase (A&A Biotechnology).

Expression and Purification. pGEX-5T-Vgb was transformed into *E. coli* BL21 (DE3). Expression of the wild-type protein was done at the 9 L scale in LB medium in a Techfors S biofermentor. Bacteria were grown at 37 °C to A_{600}= 0.9, cooled to 16 °C and induced with 0.1 mM isopropyl-β-D-thiogalactopyranoside (IPTG). Twenty-four hours after induction, cells were harvested by centrifugation. Mutant proteins were expressed similarly on a 2 L scale in shaker flask cultures.

Protein Purification. Cells were resuspended in a buffer C (50 mM HEPES at pH 7.5, 200 mM NaCl, and 10% glycerol) and treated with lysozyme, DNase I, and phenylmethylsulfonyl fluoride for 3 h at 4 °C. After sonication and centrifugation at 145,000*g*, the supernatant was applied to a Glutathione Sepharose 4B column (Amersham Bioscience) equilibrated with buffer C. The column was washed with buffer C, and the bound protein was eluted with buffer D (10 mM glutathione, 50 mM HEPES at pH 7.5, 100 mM NaCl, and 10% glycerol). To cleave off the GST-tag, the mixture was incubated in the presence of 10 mg of thrombin and 1 mM $CaCl_2$ at 4 °C for 48 h. The digestion was stopped by adding 1 mM benzamidine, and the sample was concentrated by ultrafiltration (Vivaspin, 10 kDa cutoff). The concentrated sample was subjected in several portions to gel filtration in buffer E (50 mM HEPES at pH 7.5, 10% glycerol) on a Sephacryl S-300 column (Amersham Bioscience). Although the Vgb peak of the eluate was already largely free of GST contamination, any residual GST was removed by applying the sample to a column with a fresh batch of Glutathione Sepharose 4B. The flow-through of this column was concentrated again and then subjected to a final round of gel filtration, this time on Sephacryl S-200 column (Amersham Bioscience). The peak fractions were concentrated by ultrafiltration (Vivaspin, 10 kDa cutoff) to a final concentration of 10 mg/mL. Gel filtration experiments were done at 18 °C; all other purification steps were carried out at 7 °C.

Analytical Gel Filtration. The molecular mass of *S. cohnii* Vgb was estimated by analytical gel filtration on a Superdex 75 10/300 GL column in buffer E. The experiment was repeated twice. The Vgb peak was collected and reinjected. The column was calibrated with Bio-Rad protein standards (vitamin B 12, 1.35 kDa; myoglobin, 17 kDa and ovalbumin 44 kDa). As an additional protein standard, BSA (69 kDa) was used.

CD-Spectroscopy. The effect of point mutations on protein folding was assessed by circular dichroism spectroscopy. Spectra of the wild-type and mutant proteins were recorded with a Jasco J-810 spectrometer equipped with a thermostatted cell holder and 0.02 cm sample cell. For every protein variant, three spectra (in the wavelength range from 260 to 200 nm) were recorded and averaged.

In vitro Activity Assay. Spectrophotometric and fluorometric assays of *S. aureus* streptogramin lyase activity have been reported previously (*19, 21*). The fluorometric assay (*21*) with minor modifications was used. A Shimadzu spectrofluorophotometer (Model RF-5301 PC) and 1 mL cuvette were used throughout. Quinupristin absorption was maximal at 333 nm; therefore, the fluorescence was excited at this wavelength (slit settings 3 nm). Vgb catalyzed quinupristin linearization was monitored by a decrease in the fluorescence emission at 406 nm (slit settings 10 nm). As some decrease of fluorescence with time was observed also in the absence of Vgb, a constant background drift had to be subtracted from all readings.

Reactions for Michaelis–Menten kinetics were done at 37 °C in buffer E supplemented with 1 mM $MgCl_2$ or alternatively with 10 mM EDTA. Vgb and its variants were used at 15 nM concentration (except for the H228A mutant where 30 nM of enzyme was applied). The K_m values were derived by hyperbolic regression analysis from the dependence of the initial velocity on substrate concentration (program Hyper, version 1.1s, 1996). For the determination of k_{cat} values, rates of fluorescence change were converted to reaction rates. The calibration curve was based on the assumption that the reaction had run to completion (all quinupristin was linearized) when the fluorescence changed no further. Values for k_{cat} were then calculated from the initial velocity and the known concentration of *S. cohnii* Vgb.

Protein Crystallization, Crystal Derivatization, and Data Collection. S. cohnii Vgb crystals were grown by the vapor diffusion method in sitting drops at 6 °C. Reservoir buffer F (0.1 M HEPES at pH 7.5, 0.2 M $CaCl_2$, 25% PEG 3350), 1.2 μL, was mixed with 0.4 μL 10 mM L-cysteine and 2 μL of 10 mg/mL Vgb in buffer E. Needle-like crystals appeared after 3 days. Native data were collected at the synchrotron beamline BW6 at the Deutsches Elektronensynchrotron DESY in Hamburg and were integrated and scaled with DENZO and SCALEPACK (*23*). For derivatization, native crystals were either soaked for 7 days with 2 mM $HgCl_2$ or for 1 min with 0.35 M KI at 6 °C. Diffraction data for these crystals were collected on an in-house rotating anode generator equipped with a MAR345 image plate. These data were processed with MOSFLM (*24*) and SCALA (*25*). The data for the mercury derivative extended only to 2.7 Å, but the data for the iodide soak reached to 1.8 Å and were of

Table 1: Data Collection and Refinement Statistics

Data Collection Statistics (12.0 – 1.8 Å)	
space group	*P*2(1)2(1)2(1)
a (Å)	60.5
b (Å)	68.1
c (Å)	73.2
wavelength (Å)	1.54
total reflections	96, 127
unique reflections	27, 602
completeness (%) (last shell)	96.6 (92.8)
I/σ (last shell)	16.9 (5.3)
R(sym) (%) (last shell)	3.9 (13.9)
B(iso) from Wilson (Å^2)	13.5

Refinement Statistics (12.0 − 1.8 Å)	
protein atoms (excluding H)	2315
solvent molecules	261
R-factor (%)	18.0
R-free (%)	21.5
rmsd bond lengths (Å)	0.014
rmsd angles (°)	1.3
Ramachandran core region (%)	90.2
Ramachandran allowed region (%)	9.4
Ramachandran additionally allowed region (%)	0.4
Ramachandran disallowed region (%)	0.0

better quality than synchrotron data for the native crystal. Therefore, the diffraction data for the KI soak was used for the final refinement (Table 1).

Structure Determination. Difference Patterson maps for the KI soak showed clear peaks in the Harker sections, which were readily interpreted by the RSPS program (*26*) in terms of two I^- sites located at the fractional coordinates (0.781, 0.204, 0.226) and (0.968, 0.253, 0.115), respectively. The resulting single isomorphous replacement (SIR) phases were then used for cross-phasing to interpret the $HgCl_2$ versus native difference Fourier maps in terms of two confident Hg^{2+} sites at (0.310, 0.263, 0.778) and (0.037, 0.751, 0.316). Joint MIR phasing with the program MLPHARE (*25*) (up to a resolution of 2.5 Å) indicated that for this resolution range, the average figure of merit (FOM) for centric reflections was 0.60 and for acentric reflections was 0.38, which resulted in an average figure of merit of 0.41 for all reflections in this resolution range. The phases were then extended to the full 1.8 Å resolution using the density modification program DM (*25*). In this procedure, FOM (for the full resolution range up to 1.8 Å) went up from 0.14 to 0.64 (corresponding to an increase in the correlation of the map with the final $2Fo - Fc$ map from 0.43 to 0.55). Nevertheless, the phases after solvent flattening were still of insufficient quality for automatic model building. Therefore, the modeling program O (*27, 28*) was used to assemble a first version of the *S. cohnii* Vgb structure manually. Although the resulting crude model had very poor stereochemistry and could not be refined further, it was already sufficiently accurate to scan the Protein Data Bank (PDB) for similar structures with the help of the DALI Web-server (*29, 30*). At the time (October 22nd, 2006), our preliminary *S. cohnii* Vgb model was most similar to the structure of a 7-bladed β-propeller fragment of the transcriptional cosuppressor protein TUP1 (residues 333–383, 441–565, 573–604 and 621–710). Therefore, a polyalanine version of this model was first manually superimposed on the *S. cohnii* Vgb model and then broken down into short, rigid segments. The fragments, which contained only a few consecutive β-strands each, were manually adjusted for an optimal fit to the density. After the correction of some loops, this database-guided model of *S. cohnii* Vgb was sufficiently accurate for further automatic density improvement and model building using the ARP/wARP protocol (*31*). The model was completed manually and refined with the REFMAC program (*32*).

RESULTS AND DISCUSSION

S. cohnii Vgb Expression and Purification. A Staphylococcus strain harboring the *S. cohnii vgb* gene was obtained from the collection of the Pasteur Institute in Paris, France. The gene was amplified by PCR and cloned into pGEX-5T. The resulting plasmid, pGEX-5T-Vgb, was ampicillin-selectable and directed the heterologous expression of soluble Vgb with an N-terminal, thrombin-cleavable GST-tag in *E. coli*. The recombinant protein was purified by glutathione-*S*-transferase (GST) affinity chromatography and gel filtration. Thrombin-cleavage of the N-terminal GST-tag left residues GSEAW as a cloning artifact at the N-terminus. Analytical gel filtration experiments indicated a molecular mass of 36 ± 6 kDa, consistent within the error limit with a calculated Vgb monomer mass of 33 kDa (Figure 2A and B).

S. cohnii Vgb Crystallization and Structure Determination. Crystals of *S. cohnii* Vgb were grown by the sitting drop vapor diffusion technique. Orthorhombic crystals in space group *P*2(1)2(1)2(1) appeared in the presence or absence of quinupristin and/or milimolar concentrations of divalent metal cations and contained a single molecule of Vgb in the asymmetric unit. As the *S. aureus* Vgb structure was not available at the time, attempts to solve the *S. cohnii* Vgb structure by molecular replacement (MR) were unsuccessful. The structure was eventually solved by a combination of multiple isomorphous replacement (MIR) and database-guided manual model building (see Experimental Procedures), but could of course have been solved more easily by conventional molecular replacement after the model for *S. aureus* Vgb became available. The final refinement statistics are summarized in Table 1.

A Seven-Bladed β-Propeller with a Velcro. On the basis of the presence of six readily detectable repeats in the Vgb sequence and weak similarity to the sensor domain of the *Mycobacterium tuberculosis* receptor serine/threonine protein kinase PknD, modeling programs predicted Vgb to form a six-bladed β-propeller. However, it became clear early in model building that there was an extra blade, which consisted of the first N-terminal and the three last C-terminal β-strands with their connecting loops (Figure 3A). In retrospect, this latched or Velcro arrangement could have been anticipated because it was previously observed for many other β-propeller proteins (*33*). The seven blades in the *S. cohnii* Vgb β-propeller are connected by hairpins (except for the Velcro). Within each blade, the distance of strands from the pseudo-7-fold axis increases from the N-terminus to the C-terminus (Figure 3A). Superposition shows that the seven propeller blades of *S. cohnii* Vgb are structurally very similar (Figure 3C). Excluding the discontinuous seventh blade, the average distance between Cα-atoms for an optimal superposition of blades is between 0.49 Å (blades 4 and 5) and 1.20 Å (blades 4 and 6), with an average of 0.80 Å over all pairs of blades. At least in part, this high structural similarity is attributable to the high sequence similarity between the blades. A

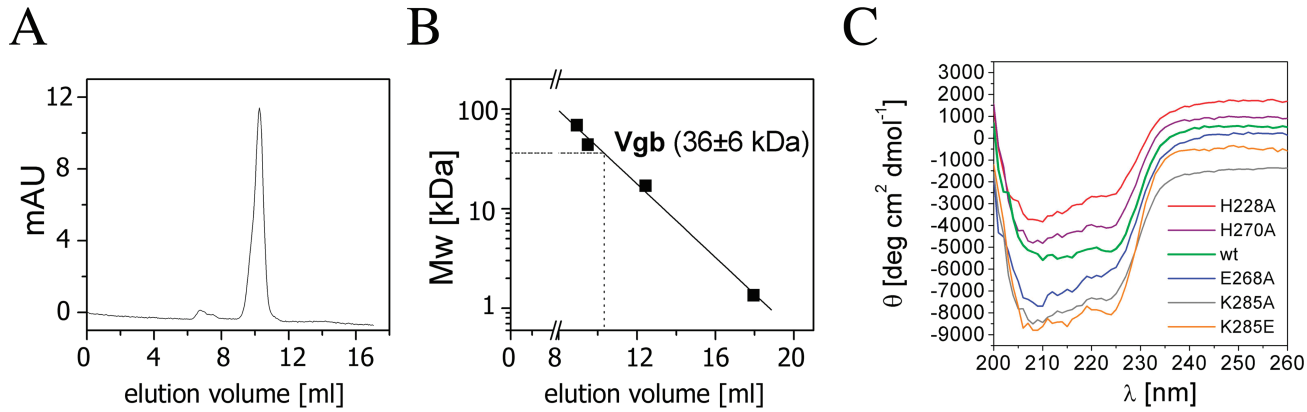

FIGURE 2: *S. cohnii* Vgb molecular mass and secondary structure content. (A) Elution profile of *S. cohnii* wild-type Vgb on a Superdex 75 gel filtration column. The Vgb peak was collected and reinjected. The retention times were 25.6 and 26.0 min, respectively. (B) Calibration curve. The column was calibrated with Bio-Rad protein standards (vitamin B 12, 1.35 kDa; myoglobin, 17 kDa and ovalbumin, 44 kDa). As an additional protein standard, BSA (69 kDa) was used. Assuming a linear dependence of the logarithm of the molecular mass on the elution time, the *S. cohnii* Vgb molecular mass was calculated as 36 ± 6 kDa. Within the error, this is consistent with a calculated monomer mass of 33 kDa. (C) Mean residue molar ellipticity versus wavelength for wild-type and variant *S. cohnii* Vgb proteins. The CD-spectrum of the wild-type protein (green) is shown as recorded. For clarity, the spectra of the H228A (red) and H270A (purple) Vgb variants have been upshifted by 2,000 and 1,000 deg cm^2 dmol^{-1}, respectively, and the spectra of the E268A (blue), K285A (gray) and K285E (orange) Vgb variants have been downshifted by 1,000 and 2,000 and 3,000 deg cm^2 dmol^{-1}, respectively.

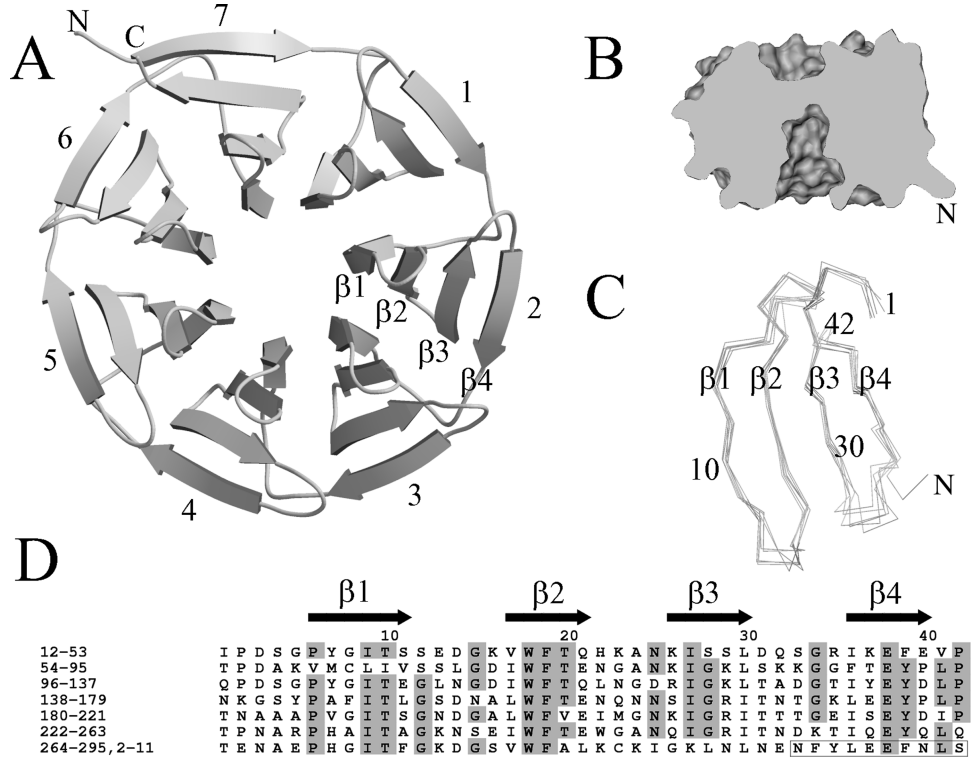

FIGURE 3: *S. cohnii* Vgb structure and sequence. (A) Secondary structure representation of the entire 7-bladed β-propeller. Each blade consists of four β-strands connected by hairpins. The N-terminal residues GSEAW, which were added to the *S. cohnii* sequence by a cloning artifact, are not shown in this model. (B) Surface representation of Vgb sliced by a plane that contains the pseudo-7-fold axis of Vgb. The view in panel A is towards what is the bottom of Vgb in panel B. (C) Superposition of the seven blades in Cα-representation. The numbering of residues is according to their position within a blade. The superimposed blades are roughly oriented like a Vgb blade close to the slicing plane on the right side of panel B. (D) Alignment of the seven repeats in the *S. cohnii* Vgb amino acid sequence. The sequence of blade 1 is at the top, and the sequence of blade 7 is at the bottom. The secondary structure information was derived from the crystal structure using the program STRIDE (*37*) and applies to blades 1 to 6. Secondary structures in blade 7 differ slightly. Strongly conserved residues are marked by gray boxes. The N-terminal part of the Vgb molecule in blade 7 is boxed.

pairwise comparison of blade sequences shows that on average 16 of the 42 blade residues (or 38%) are identical between any two blades (Figure 3D). Pairwise sequence identity is highest between blades 4 and 5 (21 identical residues or 50% identity) and lowest between blades 1 and 6 (12 identical residues or 29% identity). Only three residues are strictly conserved in all blades of *S. cohnii* Vgb: these residues are a tryptophan and a phenylalanine in strand 2 and a glutamate in strand 4. In the structure, the conserved tryptophans are located at the interfaces to the next blades (along the sequence) and the phenylalanine residues map to the interfaces with the previous blades (along the sequence). The conserved glutamates in the most C-terminal β-strand of each blade interact with a residue at the very N-terminal

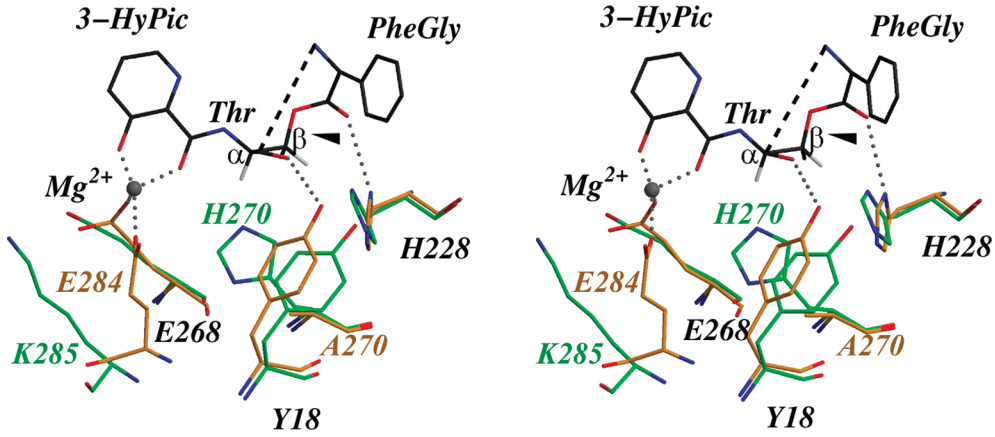

FIGURE 4: Superposition of the *S. cohnii* and *S. aureus* Vgb active sites in stereo representation. The *S. cohnii* Vgb active site residues (green) were optimally superimposed on their counterparts in the complex of inactive *S. aureus* Vgb protein variant (orange) with quinupristin (black). Quinupristin is shown in wireframe representation, with the usual color code (red for oxygen atoms, blue for nitrogen atoms). 3-HyPic stands for 3-hydroxypicolinyl, Thr stands for threonyl, and PheGly stands for phenylglycyl. The Cγ atom of threonine is difficult to see because it points away from the viewer and into the page. The Cα and Cβ carbon atoms of the threonyl residue are labeled α and β, respectively. Hydrogen atoms directly connected to these two carbon atoms are shown in gray in their inferred positions; all other hydrogen atoms are implicit. The black triangle marks the carbon−oxygen bond that breaks during catalysis. The dashed black line represents four amino acid residues of quinupristin that connect the threonyl residue to the phenylglycyl residue. Dotted gray lines indicate metal–ligand interactions or hydrogen bonds for which a role in catalysis has been suggested. Note that the H270A mutant of *S. aureus* Vgb was used for cocrystallization with quinupristin and that in wild-type *S. aureus* Vgb, a histidine residue is present just as in *S. cohnii* Vgb. The Mg^{2+} ion, which is represented by a gray ball, is present only in the *S. aureus* Vgb−quinupristin complex, but not in the *S. cohnii* Vgb structure. Also note that the model is consistent with *anti*-elimination and the formation of the Z-product (methyl and amino groups on the same side of the double bond), as required by the experimental data for *S. aureus* Vgb (*19*). The residues that are different for the two structures are marked according to the colors of the C−C bonds for the appropriate structure (green for *S. cohnii* Vgb and orange for the *S. aureus* Vgb); the labels that apply to both structures are black.

end of the blade (or for other possible choices of the blade boundary, with a residue at the very C-terminal end of the previous blade).

Active Site Near the Pseudo-7-fold Axis, on the Flat Side of Vgb. Like many other β-propeller proteins, Vgb is cup-shaped with a deep central channel on the propeller axis, which is open to one (bottom of Figure 3B), but not the other side (top of Figure 3B, see also Supporting Information, Figure 1). At first, the deep channel on the propeller axis looked like a probable quinupristin binding site (Supporting Information, Figure 1A and B). However, residue conservation scores mapped to the protein surface (compare Supporting Information, Figure 1C and D) suggested that quinupristin was more likely to bind to the opposite side of Vgb, which is fairly flat with only a shallow depression (Supporting Information, Figure 1C and D). A literature survey confirmed that this binding mode was well-documented for six-bladed β-propeller proteins (*34*) and importantly also for *Neurospora crassa* CMLE, a seven-bladed β-propeller protein that catalyzes the conversion between 3-carboxy-*cis,cis*-muconate and its lactone form. Therefore, we expected Vgb to bind substrate near the pseudo-7-fold axis on the flat side of the molecule, which was confirmed when the cocrystal structure of an inactive *S. aureus* Vgb variant with quinupristin was published (*21*). In the *S. cohnii* crystals, the Vgb active site is blocked by residues GSEAWMNFY (residues GSEAW are only present in the recombinant protein) of the N-terminus of a neighboring molecule in the crystal (Supporting Information, Figure 2). In retrospect, it is clear that this crystal contact interferes with quinupristin binding, and explains the failure of our quinupristin soaking experiments. As Mg^{2+} binding to Vgb is comediated by the Vgb substrate (*21*), it is also clear why soaking experiments with either Mg^{2+}, Mn^{2+} or Ca^{2+} ions were unsuccessful.

Predicted Active Site of S. cohnii Vgb. Substantial mechanistic similarities between the Vgb and CMLE catalyzed reactions in the ring opening direction (ignoring different metal dependencies and stereochemical courses of the β-elimination reactions) (Figure 1) and quantitative similarities between the *S. cohnii* Vgb and CMLE structures (DALI Z-score 27) suggested possible mechanistic similarities. In CMLE, His148 catalyzes the abstraction/addition of a Cα-proton in the ring opening/closing direction of the reaction. CMLE His148 has no direct counterpart in the equivalent blade of *S. cohnii* Vgb, but we noted two histidines, His228 and His270, in roughly equivalent locations in other blades of *S. cohnii* Vgb and found catalytic defects when we changed these residues to alanines (see below). Although it is now clear that the similarity of the Vgb and CMLE active sites is not due to divergent evolution (*21*), the functional equivalence of CMLE His148 and Vgb His270 was confirmed when the a cocrystal structure and detailed biochemical characterization of *S. aureus* Vgb appeared in press (*21*). This work also showed that His228 had a separate catalytic role and described additional active site residues in *S. aureus* Vgb. With the exception of Glu284 (Lys285 in *S. cohnii*), all identified *S. aureus* Vgb active site residues have direct counterparts (with identical residue numbers) in *S. cohnii* Vgb. Superposition of the *S. cohnii* and *S. aureus* Vgb structures further shows that conserved residues are present in spatially conserved locations (Figure 4). Therefore, the catalytic roles of active site residues proposed by Korczynska et al. for *S. aureus* Vgb (*21*) are likely to apply to *S. cohnii* Vgb as well. According to Korczynska et al., His270 abstracts a proton from the

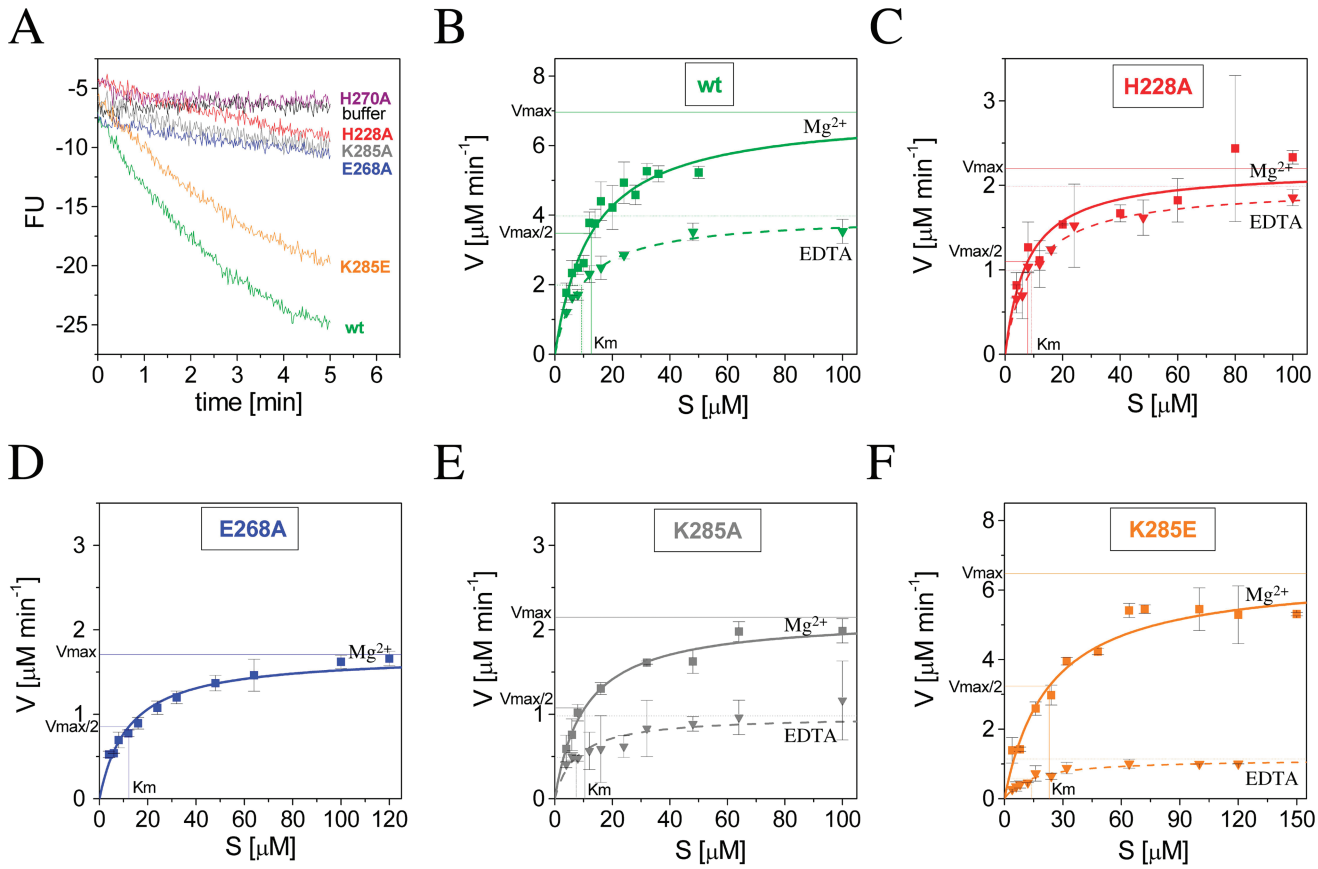

FIGURE 5: Characterization of *S. cohnii* Vgb. The *S. cohnii* Vgb mediated quinupristin linearization reduces the fluorescence of the depsipeptide. (A) Raw recordings of fluorescence versus time for the quinupristin linearization by wild-type Vgb (green), the H228A (red), H270A (purple), E268A (blue), K285A (gray), and K285E (orange) Vgb variant or buffer alone (black). (B−F) Dependence of the initial reaction velocity on the substrate concentration. Experiments were done with 15 nM of the enzyme, except for the H228A mutant protein, which was used in twice higher concentration. Reaction mixtures contained either 1 mM Mg^{2+} (squares) or 10 mM EDTA (inverted triangles). As quinupristin fluorescence is expected to be metal dependent, separate calibration curves were obtained for the conversion of fluorescence units (FU) to concentrations of linearized quinupristin for Mg^{2+} and for EDTA (Supporting Information, Figure 3).

threonyl Cα-atom when the reaction proceeds in the ring-opening direction. His228 donates a hydrogen bond from its Nδ-atom to the carbonyl oxygen atom of the phenylglycyl residue in quinupristin, which should lower the pK_a of the (conjugate acid of) the phenylglycyl residue and make it a better leaving group. Tyr18 donates a hydrogen bond to the carbonyl oxygen atom of the threonyl residue in quinupristin to stabilize the negative charge that delocalizes in part to the oxygen atom after abstraction of the Cα-proton. Glu268 is involved in metal chelation in the *S. aureus* enzyme and is predicted to have an analogous role in the *S. cohnii* enzyme (Figure 4). Another *S. aureus* Vgb active site residue, Glu284, is also involved in metal chelation and cannot be mutated to alanine without drastic loss of activity. Although this residue is highly conserved in other Vgb sequences, it is not present in *S. cohnii* Vgb. Becaue of insertions and deletions in flanking loops, the spatial equivalent of *S. aureus* Vgb Glu284 is *S. cohnii* Vgb Lys285, a residue not suitable for direct metal chelation (Figure 4). The substitution is unlikely to be a cloning artifact because wild-type *S. cohnii* Vgb with the lysine has kinetic parameters very similar to those of wild-type *S. aureus* Vgb, despite the substitution (see below).

S. cohnii Vgb Active Site Mutations. Alteration of *S. aureus* His228 or His270 reduces the activity to undetectable levels, and alterations of other active site residues result in at least a 40-fold reduction of the k_{cat}/K_m value (*21*). We therefore tested whether equivalent mutations in *S. cohnii* had similar effects on the activity. The H228A, E268A, H270A, K285A and K285E Vgb variants were expressed and purified in a manner analogous to that used with the wild-type protein. Circular dichroism spectra of all mutant proteins resembled the spectrum of the wild-type protein, indicating that the mutant proteins did not have gross folding defects (Figure 2C). Quinupristin lactone ring opening at 37 °C was followed by monitoring the accompanying decrease in fluorescence intensity essentially as previously described (*19, 21*). For all measurements, a reproducible background decrease in fluorescence had to be subtracted. Rates of fluorescence change were converted to reaction rates using the calibration curves recorded in the appropriate buffer (Supporting Information, Figure 3). For the determination of these curves, it was assumed that the reaction had proceeded to completion when no further change of fluorescence was observed. In the presence of 1 mM Mg^{2+}, the activity of 15 nM wild-type *S. cohnii* Vgb was readily detectable on a time scale of minutes (Figure 5A and B). In contrast, no activity was observed for the H270A variant of *S. cohnii* Vgb, even when the concentration of the mutant protein was increased far beyond the concentration required to observe a robust reaction for the wild-type protein. In order to distinguish whether the H270A variant was defective in substrate binding or catalysis, a competition experiment with the mutant and wild-type protein was set up. High concentrations of the *S.*

Table 2: Kinetic Constants for Wild-Type and Mutant Vgb Proteins in the Presence of 1 mM Mg^{2+} Ions or 10 mM EDTA

	1 mM $MgCl_2$			10 mM EDTA		
	K_m [μM]	k_{cat} [1/s]	k_{cat}/K_m [$M^{-1}s^{-1}$]	K_m [μM]	k_{cat} [1/s]	k_{cat}/K_m [$M^{-1}s^{-1}$]
Vgb wt	13 ± 4	7.8 ± 1.2	$6.0 \cdot 10^5$	9 ± 2	4.4 ± 0.3	$4.9 \cdot 10^5$
Vgb H228A	8 ± 5	1.2 ± 0.3	$1.5 \cdot 10^5$	9 ± 3	1.1 ± 0.2	$1.2 \cdot 10^5$
Vgb E268A	12 ± 3	1.9 ± 0.2	$1.6 \cdot 10^5$	n. m.[a]	n. m.	n. m.
Vgb H270A	–	–	–	–	–	–
Vgb K285A	10 ± 2	2.4 ± 0.2	$2.4 \cdot 10^5$	8 ± 5	1.1 ± 0.2	$1.4 \cdot 10^5$
Vgb K285E	23 ± 10	7.2 ± 1.4	$3.1 \cdot 10^5$	14 ± 4	1.2 ± 0.1	$0.9 \cdot 10^5$

[a] n. m., not measured.

cohnii Vgb H270A variant but not of the control protein bovine serum albumin protected quinupristin against the activity of the wild-type protein (Supporting Information, Figure 4). This result is consistent with a catalytic defect of the H270A variant, but could also be explained by a direct inhibitory effect of the mutant protein on the wild-type protein, especially in light of the crystallographic information. With the exception of the *S. cohnii* Vgb H270A variant, the mutant proteins had sufficient activity for the determination of K_m and k_{cat} values assuming standard Michaelis–Menten kinetics (Figure 5 and Table 2). The K_m and k_{cat} values for wild-type *S. cohnii* Vgb (Figure 5B) were very similar to the previously reported values for *S. aureus* Vgb (*21*). The same was true for the *S. cohnii* Vgb K285E variant (Figure. 5F), which was made to mimic the active site of wild-type *S. aureus* Vgb. As expected, all other mutations impaired catalytic activity (Figures 5C−E and Table 2). The H270A mutation abolished activity entirely, as previously reported for the *S. aureus* enzyme by Korczynska et al. (*21*). All other mutations had milder effects in our assays than those reported by Korczynska et al. for the *S. aureus* enzyme, perhaps indicating a genuine difference between the *S. aureus* and *S. cohnii* enzymes. Contamination of our enzyme preparations with background lyase activity might have been an alternative explanation, but was unlikely because no residual activity was detected for the H270A mutant of *S. cohnii* Vgb, which was purified according to the same protocol.

In contrast to the strict metal dependence of *S. aureus* Vgb (*19*), a substantial residual activity of *S. cohnii* wild-type Vgb was detectable in the absence of exogenously added Mg^{2+} ions. This residual activity persisted when quinupristin and Vgb were separately preincubated with 10 mM EDTA at 4 °C for at least 12 h (Figure 5B). This result could indicate that Mg^{2+} ions remained chelated by quinupristin, explaining why against expectation (*35*) similar calibration curves were obtained in the presence of 1 mM Mg^{2+} and in the presence of 10 mM EDTA (Supporting Information, Figure 3). Alternatively, *S. cohnii* Vgb is less metal dependent than *S. aureus* Vgb, perhaps because the charged ϵ-amino group of Lys285 could functionally substitute for the metal ion. This interpretation is supported by the strong metal dependence of the *S. aureus* Vgb-like *S. cohnii* K285E variant (Figure 5F) but remains to be reconciled with the substantial residual activity of the *S. cohnii* Vgb K285A variant in the presence of EDTA (Figure 5E). Together, our data suggest that *S. cohnii* Vgb is more tolerant toward modifications of the metal chelating residues than *S. aureus* Vgb because its activity is only partially dependent on the presence of divalent metal ions. This difference aside, our data support the novel catalytic mechanism that has been proposed (*21*) to account for the mechanistically remarkable opening of a lactone-ring by β-elimination.

ACKNOWLEDGMENT

We thank the staff of the Pasteur Institute for *S. aureus* sp. *aureus* strain BM12392-I1877 that contains plasmid pIP1714 with the *vgb* gene, Henryk Korza for his early work on the project, and Dr. Honorata Czapinska and Dr. Aneta Kaczmarczyk for proofreading the manuscript.

SUPPORTING INFORMATION AVAILABLE

Surface representation of *S. cohnii* Vgb colored according to electrostatic potential and amino acid conservation. Stereo view of the *S. cohnii* Vgb active site with quinupristin modeled into the crystal structure of *S. cohnii* Vgb without substrate and with the N-terminus of a neighboring molecule in the crystal inserted into the active site. Calibration curve for kinetic measurements. Competition of the *S. cohnii* Vgb H270A mutant with wild-type enzyme. This material is available free of charge via the Internet at http://pubs.acs.org.

REFERENCES

1. Livermore, D. M. (2000) Quinupristin/dalfopristin and linezolid: where, when, which and whether to use. *J. Antimicrob. Chemother. 46*, 347–350.
2. Johnson, A. P., and Livermore, D. M. (1999) Quinupristin/dalfopristin, a new addition to the antimicrobial arsenal. *Lancet 354*, 2012–2013.
3. Rubinstein, E., Prokocimer, P., and Talbot, G. H. (1999) Safety and tolerability of quinupristin/dalfopristin: administration guidelines. *J. Antimicrob. Chemother. 44*, 37–46.
4. Pankuch, G. A., Kelly, L. M., Lin, G., Bryskier, A., Couturier, C., Jacobs, M. R., and Appelbaum, P. C. (2003) Activities of a new oral streptogramin, XRP 2868 compared to those of other agents against *Streptococcus pneumoniae* and *Haemophilus* species. *Antimicrob. Agents Chemother. 47*, 3270–3274.
5. Tu, D., Blaha, G., Moore, P. B., and Steitz, T. A. (2005) Structures of MLSBK antibiotics bound to mutated large ribosomal subunits provide a structural explanation for resistance. *Cell 121*, 257–270.
6. Harms, J. M., Schlunzen, F., Fucini, P., Bartels, H., and Yonath, A. (2004) Alterations at the peptidyl transferase centre of the ribosome induced by the synergistic action of the streptogramins dalfopristin and quinupristin. *BMC Biol. 2*, 4.
7. Mukhtar, T. A., and Wright, G. D. (2005) Streptogramins, oxazolidinones, and other inhibitors of bacterial protein synthesis. *Chem. Rev. 105*, 529–542.
8. Allington, D. R., and Rivey, M. P. (2001) Quinupristin/dalfopristin: a therapeutic review. *Clin. Ther. 23*, 24–44.
9. Cocito, C. (1979) Antibiotics of the virginiamycin family, inhibitors which contain synergistic components. *Microbiol. Rev. 43*, 145–192.
10. Allignet, J., Loncle, V., Simenel, C., Delepierre, M., and el Solh, N. (1993) Sequence of a staphylococcal gene, vat, encoding an acetyltransferase inactivating the A-type compounds of virginiamycin-like antibiotics. *Gene 130*, 91–98.
11. Allignet, J., Liassine, N., and el Solh, N. (1998) Characterization of a staphylococcal plasmid related to pUB110 and carrying two

novel genes, vatC and vgbB, encoding resistance to streptogramins A and B and similar antibiotics. *Antimicrob. Agents Chemother. 42*, 1794–1798.
12. Kehoe, L. E., Snidwongse, J., Courvalin, P., Rafferty, J. B., and Murray, I. A. (2003) Structural basis of Synercid (quinupristin-dalfopristin) resistance in Gram-positive bacterial pathogens. *J. Biol. Chem. 278*, 29963–29970.
13. Allignet, J., and El Solh, N. (1999) Comparative analysis of staphylococcal plasmids carrying three streptogramin-resistance genes: vat-vgb-vga. *Plasmid 42*, 134–138.
14. Allignet, J., Loncle, V., and el Sohl, N. (1992) Sequence of a staphylococcal plasmid gene, vga, encoding a putative ATP-binding protein involved in resistance to virginiamycin A-like antibiotics. *Gene 117*, 45–51.
15. Monod, M., Denoya, C., and Dubnau, D. (1986) Sequence and properties of pIM13, a macrolide-lincosamide-streptogramin B resistance plasmid from *Bacillus subtilis*. *J. Bacteriol. 167*, 138–147.
16. Bussiere, D. E., Muchmore, S. W., Dealwis, C. G., Schluckebier, G., Nienaber, V. L., Edalji, R. P., Walter, K. A., Ladror, U. S., Holzman, T. F., and Abad-Zapatero, C. (1998) Crystal structure of ErmC′, an rRNA methyltransferase which mediates antibiotic resistance in bacteria. *Biochemistry 37*, 7103–7112.
17. Allignet, J., Loncle, V., Mazodier, P., and el Solh, N. (1988) Nucleotide sequence of a staphylococcal plasmid gene, vgb, encoding a hydrolase inactivating the B components of virginiamycin-like antibiotics. *Plasmid 20*, 271–275.
18. Bateman, K. P., Yang, K., Thibault, P., White, R. L., and Vining, L. C. (1996) Inactivation of etamycin by a novel elimination mechanism in *Streptomyces lividans*. *J. Am. Chem. Soc. 118*, 5335–5338.
19. Mukhtar, T. A., Koteva, K. P., Hughes, D. W., and Wright, G. D. (2001) Vgb from *Staphylococcus aureus* inactivates streptogramin B antibiotics by an elimination mechanism not hydrolysis. *Biochemistry 40*, 8877–8886.
20. Kajander, T., Merckel, M. C., Thompson, A., Deacon, A. M., Mazur, P., Kozarich, J. W., and Goldman, A. (2002) The structure of *Neurospora crassa* 3-carboxy-cis,cis-muconate lactonizing enzyme, a beta propeller cycloisomerase. *Structure 10*, 483–492.
21. Korczynska, M., Mukhtar, T. A., Wright, G. D., and Berghuis, A. M. (2007) Structural basis for streptogramin B resistance in *Staphylococcus aureus* by virginiamycin B lyase. *Proc. Natl. Acad. Sci. U.S.A. 104*, 10388–10393.
22. Berthold, H., Frorath, B., Scanarini, M., Abney, C. C., Ernst, B., and Northemann, W. (1992) Plasmid pGEX-5T: An alternative system for the expression and purification of recombinant proteins. *Biotechnol. Lett. 14*, 245–250.
23. Otwinowski, Z., and Minor, W. (1997) Processing of X-ray diffraction data collected in oscillation mode. *Methods Enzymol. 276*, 307–326.
24. Leslie, A. W. G. (1992) Recent changes to the MOSFLM package for processing film and image plate data, Joint CCP4 + ESF-EAMCB Newsletter on Protein Crystallography 26.
25. Collaborative Computational Project Number 4. (1994) The CCP4 Suite: Programs for Protein Crystallography, *Acta Crystallogr., Sect. D 50*, 760–763.
26. Knight, S. D. (2000) RSPS version 4.: a semi-interactive vector-search program for solving heavy-atom derivatives. *Acta Crystallogr., Sect. D 56*, 42–47.
27. Jones, T. A., Zou, J. Y., and Cowan, S. W. (1991) Improved methods for building protein models in electron density maps and the location of errors in these models. *Acta Crystallogr., Sect. A 47*, 110–119.
28. Kleywegt, G. J., and Jones, T. A. (1998) Databases in protein crystallography. *Acta Crystallogr., Sect. D 54*, 1119–1131.
29. Holm, L., and Sander, C. (1993) Protein structure comparison by alignment of distance matrices. *J. Mol. Biol. 233*, 123–138.
30. Holm, L., and Sander, C. (1995) Dali: a network tool for protein structure comparison. *Trends Biochem. Sci. 20*, 478–480.
31. Morris, R. J., Perrakis, A., and Lamzin, V. S. (2003) ARP/wARP and automatic interpretation of protein electron density maps. *Methods Enzymol. 374*, 229–244.
32. Murshudov, G. N., Vagin, A. A., and Dodson, E. J. (1997) Refinement of macromolecular structures by the maximum-likelihood method. *Acta Crystallogr., Sect. D 53*, 240–255.
33. Fulop, V., and Jones, D. T. (1999) Beta propellers: structural rigidity and functional diversity. *Curr. Opin. Struct. Biol. 9*, 715–721.
34. Good, M. C., Greenstein, A. E., Young, T. A., Ng, H. L., and Alber, T. (2004) Sensor domain of the *Mycobacterium tuberculosis* receptor Ser/Thr protein kinase, PknD, forms a highly symmetric beta propeller. *J. Mol. Biol. 339*, 459–469.
35. Di Giambattista, M., Engelborghs, Y., Nyssen, E., Clays, K., and Cocito, C. (1991) Interaction between virginiamycin S and ribosomes is partly provided by a salt bridge with a Mg2+ ion. *Biochemistry 30*, 7277–7282.
36. Kirby, G. W., Loughlin, G. J., and Robins, D. J. (1975) The stereochemistry of the enzymatic cyclisation of 3-carboxymuconic acid to 3-carboxymuconolactone. *J. Chem. Soc., Chem. Commun.* 402–403.
37. Frishman, D., and Argos, P. (1995) Knowledge-based protein secondary structure assignment. *Proteins 23*, 566–579.

BI7015266